Effect of The Calcination Process On The Magnetotransport Properties in Co-Precipitation Derived La0.67Ca0.33MnO3 Ceramics

Yule Li
Kunming University of Science and Technology - Lianhua Campus: Kunming University of Science and Technology

Ping Yu
Kunming University of Science and Technology - Lianhua Campus: Kunming University of Science and Technology

Xiaojin Wang
Kunming University of Science and Technology - Lianhua Campus: Kunming University of Science and Technology

Fuxin Ling
Kunming University of Science and Technology - Lianhua Campus: Kunming University of Science and Technology

Qingming Chen
Kunming University of Science and Technology - Lianhua Campus: Kunming University of Science and Technology

Hui Zhang (harry_zhang71@163.com)
Kunming University of Science and Technology - Lianhua Campus: Kunming University of Science and Technology https://orcid.org/0000-0001-7471-5832

Research Article

Keywords: La0.67Ca0.33MnO3, TCR, MR, calcination process, co-precipitation method

Posted Date: April 3rd, 2021

DOI: https://doi.org/10.21203/rs.3.rs-376935/v1

Effect of the calcination process on the magnetotransport properties in co-precipitation derived $La_{0.67}Ca_{0.33}MnO_3$ ceramics

Yule Li, Ping Yu, Xiaojin Wang, Fuxin Ling, Qingming Chen, Hui Zhang*

Faculty of Materials Science and Engineering, Kunming University of Science and Technology, Kunming 650093, China

*E-mail: harry_zhang71@163.com

Abstract:

$La_{0.67}Ca_{0.33}MnO_3$ (LCMO) attracts considerable attention as a quintessential example for colossal magnetoresistance (*CMR*), metal-insulator transition and related temperature coefficient of resistance (*TCR*) studies. Here, co-precipitation method was utilized to prepare the LCMO ceramics, whose magnetotransport properties as a function of calcination temperature (T_{cal}) and calcination time (t_{cal}) were investigated. The magnetotransport properties of these LCMO ceramics were significantly enhanced compared with LCMO derived by sol-gel methods. The *TCR* of LCMO increased firstly and then decreased as the T_{cal} increased, whereas the metal-insulator transition temperature (T_{MIT}) shifted towards to the lower temperature. Magnetoresistance (*MR*) increased as T_{cal} rose and reached 82.4 % at T_{cal} = 800 ℃. The mechanism of such magnetotransport properties with different temperature ranges was discussed. The optimal *TCR* of 32.3%·K^{-1} in LCMO was prepared with T_{cal} = 500 ℃ and t_{cal} = 8 h, showing that co-precipitation method would facilitate the potential application of LCMO in infrared detecting and magnetoresistive switching.

Keywords: $La_{0.67}Ca_{0.33}MnO_3$; *TCR*; *MR*; calcination process; co-precipitation method.

1. Introduction

The past decades have witnessed the intensive study of manganite $R_{1-x}B_xMnO_3$ (*R*

is La, Sr, Nd *etc*., and *B* is divalent alkaline earth element) due to their rich electronic properties, which arise from interplay among lattice, spin, charge, and orbital [1] . Among them, $La_{1-x}Ca_xMnO_3$ is a typical mixed-valence compound obtained by substituting La for Ca from the parent compound, antiferromagnetic (AFM) insulator $LaMnO_3$. LCMO has been paid extensive attention, owing to the colossal magnetoresistive (*CMR*) effect and the potential applications for magnetic sensors, memory devices, *etc.*[2-5]. Furthermore, there exists a paramagnetism-ferromagnetism transition generally accompanied by a metal-insulator transition (MIT) in LCMO [6], which is well accepted as a result of competition between double exchange of Mn^{3+}/Mn^{4+} and Jahn-Teller effect [7,8]. A sharp MIT with a low resistivity can generate a large *TCR*, which makes the *CMR* manganites of great application potential in infrared detecting and bolometer, *etc*.[9,10], which motivated this study.

TCR is usually related to the grain size, crystallinity and homogeneity of the ceramic powders. These electrical and magnetotransport properties rely drastically on the preparation methods as well as preparation conditions. Many techniques can be used to prepare LCMO powders, such as the solid phase reaction [11], spray-drying [12], sol-gel method [13], co-precipitation method [14]. As for conventional solid phase reaction, a relative high calcination temperature, long calcination time and multiple grinding and sintering processes are necessary to obtain high-quality LCMO ceramics. A solution of particular concentration and a co-current flow atomization system are required of spray-drying, which increased the preparation complexity and cost. Sol-gel method also has several disadvantages, the raw materials for the sol-gel method are expensive, the operation is complicated, the process time is long and the prepared samples are prone to crack. Notice that, the chemical co-precipitation method is simple in operation and mild in condition, which is utilized in this study to prepare LCMO ceramics.

The composition and morphology of the sample can be precisely controlled by changing the calcination temperature (T_{cal}) and calcination time (t_{cal}) [15-20]. Previous studies reported the electrical properties and *TCR* of $La_{0.67}Ca_{0.33}MnO_3$, with

maximum *TCR* of 9.7%·K^{-1} and corresponding metal-insulator transition temperature (T_{MIT}) of 267.59 K [21,22]. Therefore, it is of importance to further explore different calcination process to enhance *MR* and *TCR* in co-precipitation derived LCMO ceramics.

In present work, calcination process effect on the electrical transport and magnetotransport properties of LCMO ceramics. T_{cal} of 400, 500, 650 and 800 ℃ were used since the synthesis of the LCMO phase started at about 500°C and completed at about 800 °C [21]. The maximum *TCR* reached to 32.3 %·K^{-1} at T_{cal} = 500 ℃ and maximum *MR* is 82.8 % at T_{cal} = 800 ℃, which are largely enhanced compared with the sample derived by sol-gel method [23]. In the region of $T < T_{MIT}$, the ρ-T could be demonstrated by the electron-electron scattering. In the region of $T > T_{MIT}$, conductive mechanism was explained through the small polaron hopping (*SPH*) model. In addition, the resistivity (ρ) can be fitted by phenomenological percolation model over the entire temperature scope. Our study provides a new synthesis method for the application of LCMO materials in infrared detectors, contactless magnetoresistive switches, and memories to some extent.

2. Experiments

$La_{0.67}Ca_{0.33}MnO_3$ (LCMO) ceramics were synthesized with the co-precipitation method. High purity powders ($La(NO_3)_3 \cdot nH_2O$, $Ca(NO_3)_2 \cdot 4H_2O$, $Mn(NO_3)_2 \cdot 4H_2O$, and $(NH_4)_2CO_3$) were weighed according to the stoichiometric ratio, and deionized water (approximately 50 mL) were added to the mixture. $(NH_4)_2CO_3$ powder was added to the mixed solution as a precipitator. The resulting solutions were magnetically stirred for about 40 min. Then, the samples were filtered, washed with deionized water, and the precipitates were separated from the water after standing for 14 h. The white solid powder was formed by drying in an oven at 140 °C for 6 h. The dried precipitates were calcined in a muffle furnace at 400 °C, 500 °C, 650 °C, and 800 °C. The calcined powders were ground again. To break the hard agglomerates and improve the activity of effective densification during sintering processes, the milled powder was pressed

into pellets at 15 MPa. In the ambient atmosphere, pellets were sintered in a muffle furnace at 1450 °C for 12 h. The t_{cal} was set to 0, 2, 8, and 24 h at T_{cal} = 500 ºC.

The structure and crystallinity of the LCMO samples were studied by powder X-ray difraction (*XRD,* Rigaku Ultima IV) with Cu Kα radiation. The surface morphologies and microstructures were characterized by scanning electron microscope (*SEM*, Hitachi SU8010). The resistivity was measured with the standard four probe method within a temperature range of 150-300 K. The magnetoresistance (*MR*) was measured with a magnetic measurement system within a temperature range of 150-300 K.

3. Results and discussions

3.1. Structure of LCMO samples

XRD patterns of the LCMO ceramic samples calcinated at different temperatures are shown in Fig. 1. All samples possessed the orthorhombic perovskite structure, no impurity phases. Insets showed a magnified view of the strongest diffraction peak (121), which shifted toward lower angles as the T_{cal} rose, indicating an increased volume of the unit cell. The fitting parameter values are represented in Table 1. The crystal structure of ceramic samples was orthorhombic, which space group was Pnma. The fitting parameters (a,b and c) significantly changed at different T_{cal}. The cell volume (v) increased as the T_{cal} increased from 400 ºC to 500 ºC and decreased from 500 ºC to 800 ºC. The Mn-O-Mn bond distances and Mn-O bond angles of all ceramics changed as the T_{cal} changed, which would strongly affect the transport properties.

3.2. Surface morphologies of LCMO samples

The surface morphologies of the LCMO samples are presented in Fig. 2(a-d). A large number of holes were found at the grains and grain boundaries (GBs) at T_{cal} = 400

ºC. This may be because the decomposition temperature of $Ca(OH)_2$ is in the range of 500-650 °C. The excessively low T_{cal} cannot completely decompose the $Ca(OH)_2$ in the precursor powder, and CO_2 will be generated during the calcination process, causing the pores and defects at the grains and GBs. For T_{cal} above 500 °C, fewer defects were observed, while the densities of all samples increased. To explore the effects of grain size on different T_{cal}, the mean grain sizes of all samples were calculated with Nona Measurer 1.2 Software. The average grain sizes in Fig. 2(a-e) were 13.16, 14.89, 15.05, and 25 μm, respectively. This indicates that increased T_{cal} would lead to the growth of polycrystalline ceramic grains. This is mainly because with the increase of the T_{cal}, the sample activity will increase, resulting in higher crystallinity. However, when T_{cal} was 800 °C, the grain size of the powder can reach to 25 μm and the main crystal phase is formed, reducing the sintering activity and affecting the process of secondary recrystallization. In summary, the samples have good sintering activity and few defects at a T_{cal} of 500 °C.

3.3. Electrical transport properties

The temperature dependence of the resistivity (ρ-T) of LCMO was measured in the 150-300 K under 0 and 1 T (Fig. 3(a-d)). The ρ-T curves indicated that all samples underwent a metal to insulator transition [24,25]. In the low T_{cal} region of 400-650 °C, the T_{MIT} and resistivity of LCMO ceramics showed a slight change. When T_{cal} was lifted from 650 to 800 °C, the ceramics simultaneously showed a sudden drop in T_{MIT} and a drastic increase in ρ. The reduced grain size will enlarge the surface energy. For a T_{cal} of 400-650 °C, the grain size of the LCMO powder is small (13.16, 14.89, and 15.05 μm, respectively), and the surface energy is larger than the sample of T_{cal} of 800 °C. As a consequence, the ceramics with-size grains dense and high density was obtained after sintering. The scattering effect of the GBs on the electrons was weakened inducing a low resistivity. Combined with *SEM* image analysis, the high T_{cal} of 800 °C is believed to be detrimental to the TCR.

The resistivity for all samples substantially decreased under 1T field, Helman and Abeles 's model [26] can be used to explain. This model simulated that the resistivity should flat out gradually with the increase of the magnetic field and eventually vanish at certain critical field. The ρ-T curves showed that the resistivity decreased and the T_{MIT} shifted towards the higher temperature. it will cause delocalization of charge carriers at 1T field, which may lead to the ordering of magnetic spins and decrease the resistivity.

The *TCR* of the samples prepared at different T_{cal} are shown in Fig. 3(e). The main electrical performance comparison of LCMO samples under different T_{cal} are presented in Table 2. Fig. 3(e) and Table 2 show that the peak *TCR* increased first and then decreased with the T_{cal} increased. When T_{cal} = 500 °C, the *TCR* reached 32.3%·K^{-1}, and T_{MIT} shifted toward the low-temperature region, which show the advantages over the provious studies [27,28]. The reason for this phenomenon is that the lower T_{cal} (400 - 500 °C) causes smaller-size precursor particles, produces denser ceramics, which involves fewer GBs and fewer pores, especially the latter; and boosts the transport properties. On the other hand, looser ceramics derived from higher T_{cal} (650-800 °C) can result into poorer conductivity, which is responsible for the low *TCR* observed in Fig. 3(e). However, for T_{cal} of 400 °C, the organics were not completely evaporated, which suppressed the *TCR*. In summary, optimal *TCR* can be found in the LCMO with T_{cal} of 500 °C.

Fig. 3(f) shows the MR versus temperature curves of the LCMO ceramics at 0 T and 1 T magnetic fields. In this case, the *MR* is defined as $MR = (\rho_0 - \rho_H)/\rho_0 \times 100\%$, where ρ_0 and ρ_H are the resistivity values for the 0 and 1T field, respectively. The *MR* of the LCMO ceramics can be seen as roughly increasing. The *MR* is as high as 82.4% at T_{cal} = 800 °C, which is higher than the *MR* of LCMO ceramics prepared by the sol-gel method [29,30].

3.4. Mechanism of the transport properties

There are three temperature regimes considered in this study to understand the conduction mechanism of the ρ-T of LCMO ceramics prepared by co-precipitation at different temperatures [31,32].

3.4.1 Low-temperature range

Eq. (1) is a famous empirical equation that has provided a fitting method for ρ-T in the low-temperature region ($T < T_{MIT}$):

$$\rho_{FM}(T) = \rho_0 + \rho_2 T^2 + \rho_{4.5} T^{4.5}, \qquad (1)$$

where ρ_0 is the residual resistivity stemming from the GBs, as well as from the scattering mechanisms, which independent of temperature. The $\rho_2 T^2$ is caused by the scattering of electron-electron, which plays a dominant role in the $T < T_{MIT}$ area. The $\rho_{4.5} T^{4.5}$ is produced by the electron-electron, electron-magnon, and electron-phonon scattering in the ferromagnetic (FM) low-temperature region.

The ρ-T fitted by Eq. (1) are shown in Fig. 4(a) and Table 3. The squared linear correlation coefficients (R^2) are listed. The obtained values of R^2 were as high as 99.0% for all samples, which represents the high fitting quality. With application of 1T magnetic field, it can be seen from Table 3 that both the fitting values of ρ_0 and ρ_2 for all ceramics decreased. Additionally, the GB scattering decreases, which would be resulted in decreases of resistivity. The value of the $\rho_2 T^2$ is greater than that of the $\rho_{4.5} T^{4.5}$ for all ceramics. Consequently, the scattering of electron-electron plays a major role in the conductivity of samples in the $T < T_{MIT}$ regime.

3.4.2 High-temperature range

The ρ-T of paramagnetic (PM) high-temperature region is fitted by *SPH* model. The *SPH* model could be approximated by an adiabatic Eq. (2).

$$\rho_{PM}(T) = \rho_{OS} T exp(E_a / K_b T), \qquad (2)$$

where ρ_{OS} is the resistivity coefficient, E_a is the polaron activation energy, and K_b is the Boltzmann constant.

The ρ-T fitting results are presented in Fig. 4(b) and Table 4. The results revealed that the *SPH* model fits the ρ-T well. The fitting parameters are shown in Table 4. After 1T magnetic field was applied, the E_a values of all ceramics are decreased, which would due to the addition of an external magnetic field changing the bond angle of Mn-O-Mn. In other words, the effective carrier mass is changed. As a result of this influence, the effective band gap is changed, and the carrier needs higher values of activation energy to cross this gap.

3.4.3 Entire temperature range

The phenomenological percolation model analyzed the ρ over the whole temperature scope, and the combined formula is as follows in Eq. (3).

$$\rho(T) = \rho_{FM}(T)f + \rho_{PM}(T)(1-f), \qquad (3)$$

where f is the volume fraction of the FM phase and $(1-f)$ is the volume fraction of the PM phase. LCMO ceramics has been fitted over the whole temperature scope with Eq. (3) and the fitting parameters are demonstrated in Fig. 4(c) and Table 5. *Tc-mod* stands for temperature at maximum resistivity. $\mathrm{U} \approx U_0(1 - T/T_{c-mod})$ is the energy difference between the FM and PM states. There are two adjustable fitting parameters, namely, *Tc-mod* and U_0. The fitting parameters *Tc-mod* and U_0/K_B are shown in Table 1. Obviously, the value of the *Tc-mod* is very closed to T_{MIT}.

3.5. Effect of t_{cal}

Fig. 5(a) is the ρ-T curves of LCMO with t_{cal} of 0, 2, 8, and 24 h. For t_{cal} of 0 h (that is, the temperature is lowered just after the sample is heated to 500 ºC), the resistivity is as high as 1.0412 Ω·cm, which is much higher than other study [33]. This may be that $Ca(OH)_2$ etc. are not completely decomposed, resulting in a large number of pores in the target, uneven composition, and low density, which largely improves resistivity. The resistivity of the samples reached a maximum value of 271.3 K at 8 h. From Fig. 5(b), the *TCR* first increased and then decreased. It reached a maximum value

of 32.3%·K^{-1} at t_{cal} = 8 h. In general, the T_{cal} of 500 ºC and the t_{cal} of 8 h are found to be the optimal sintering parameters for the co-precipitation derived LCMO ceramic.

4. Conclusion

A series of LCMO ceramics were prepared by co-precipitation method. The effect of calcination process on structure and magnetoelectric transport performance of LCMO ceramics was studied, and the conduction mechanism of the ρ-T was analyzed. Electron-electron scattering played an important role in the region of $T < T_{MIT}$, *SPH* dominated in the regions of $T > T_{MIT}$. Moreover, the ρ-T curves can also be interpreted by the phenomenological percolation model over the whole temperature range. Compared with sol-gel method, both *TCR* and *MR* have been greatly improved. The *TCR* maximum value is 32.3%·K^{-1} at T_{cal} = 500 °C. *MR* value reached 82.4 % at T_{cal} = 800 °C. The optimal calcination parameters are T_{cal} of 500 °C and t_{cal} of 8 h, which move forward of LCMO for infrared detecting.

Acknowledgments

This work was supported by the National Natural Science Foundation of China (No. 11564021), and the Analysis and Testing Foundation of Kunming University of Science and Technology (No. 2019P20181130001). We thank Liang Wu from Kunming University of Science and Technology for fruitful discussion.

References

[1] C.N.R. Rao, B. Raveau, Colossal magnetoresistance, charge ordering and related properties of manganese oxides, World Scientific.1998.

[2] G.H. Jonker, J.H.V. Santen, Ferromagnetic compounds of manganese with perovskite structure, Physica. 16 (1950) 337-349.

[3] R.P. Hunt, A magnetoresistive readout transducer, Ieee. T. Magn, 6 (1971) 150-154.

[4] Y. Tokura, Colossal magnetoresistive oxides, CRC Press 2000.

[5] G.Q. Gong, C. Canedy, G. Xiao, J.Z. Sun, A. Gupta, W.J. Gallagher, Colossal magnetoresistance of 1 000 000-fold magnitude achieved in the antiferromagnetic phase of $La_{1-x}Ca_xMnO_3$, Appl. Phys. Lett. 67 (1995) 1783-1785.

[5] P. Grünberg. Layered magnetic structures: interlayer exchange coupling and giant magnetoresistance, Cheminform, 26 (1995) 479-494.

[6] J. Barratt, M.R. Lees, G. Balakrishnan, D.M. Paul. Insulator–metal transitions in $Pr_{0.7}Ca_{0.3}MnO_3$ induced by a magnetic field, Appl. Phys. Lett. 68 (1996) 424-426.

[7] C. Zener. Interaction between the shells in the transition metals. Physical Review. 82 (1951) 403-405.

[8] J. Kanamori, Superexchange interaction and symmetry properties of electron orbitals,J. Phys. Chem. Solids. 10 (1959) 87-98.

[9] X. Yue, Y. Zhan, X. Liu, G. Gu, Q. Wang, X. Yin, Enhanced electrical properties of $La_{0.7}(Ca_{0.2}Sr_{0.1})MnO_3$ polycrystalline composites with Ag addition, J. Low Temp. Phys, 180 (2015) 356-362.

[10] D.H. Manha, P.T. Phong, T.D. Thanh, L.V. Hong, N.X. Phuc, Low-fifield magnetoresistance of $La_{0.7}Ca_{0.3}MnO_3$ perovskite synthesized by reactive milling method, J. Alloy. Compd. 499 (2010) 131-134.

[11] B. Vertruyen, J.-F. Fagnard, Ph. Vanderbemden, M. Ausloos, A. Rulmont,R. Cloots, Electrical transport and magnetic properties of Mn_3O_4-$La_{0.7}Ca_{0.3}MnO_3$ ceramic composites prepared by a one-step spray-drying technique, J. Eur Ceram. Soc. 27 (2007) 3923-3926.

[12] S. Mathur, H. Shen, Structural and physical properties of $La_{2/3}Ca_{1/3}MnO_3$ prepared via a modified sol-gel method, J. Sol-Gel. Sci Techn. 25 (2002) 147-157.

[13] M.L Li , M.X Xu, Effect of dispersant on preparation of barium–strontium titanate powders through oxalate co-precipitation method, Mater. Res. Bull. 44 (2009) 937-942.

[14] T Yi, S Gao, X Qi, Y.F Zhu, F.X Cheng, B.Q Ma, Y.H Huang, C.S Liao, C.H Yan, Low temperature synthesis and magnetism of $La_{0.75}Ca_{0.25}MnO_3$ nanoparticles, J. Phys Chem Solids. 61 (2000) 1407-1413.

[15] P.N. Lisboa-Filho, A.W. Mombru, H. Pardo, W.A. Ortiz, E.R. Leite, Influence of processing conditions on the crystal structure and magneticbehavior of $La_{0.7}Ca_{0.3}MnO_3$ samples, J. Phys Chem Solids. 64 (2003) 583-591.

[16] D Markovic, V Kusigerski, M Tadic, J Blanusa, Z Jaglicic, N Cvjeticanin, V Spasojevi, The influence ofthe heat treatment on the structural and magnetic properties of nanoparticle $La_{0.7}Ca_{0.3}MnO_3$ prepared by glycine-nitrate method, J. Alloy. Compd. 494 (2010) 52-57.

[17] M.H, S Baazaoui, M Hlil, E.K. Oumezzine, Mohamed, Effect of synthesis techniques on structural, magnetocaloric and critical behavior of $Pr_{0.6}Ca_{0.1}Sr_{0.3}Mn_{0.975}Fe_{0.025}O_3$ manganites, Ceram. Int. 41 (2015) 12407-12416.

[18] H.L. Ju, J. Gopalakrishnan, J.L. Pengl, Dependence of giant magnetoresistance on oxygen stoichiometry and magnetization in polycrystalline $La_{0.67}Ba_{0.33}MnO_3$, Phys. Rev. B. 51 (1995) 6143-146.

[19] S.B. Li, C.B. Wang,b, H.X. Liu, L. Li, Q. Shen, M.Z. Hu, L.M. Zhanga, Effect of sintering temperature on structural, magnetic and electrical transport properties of $La_{0.67}Ca_{0.33}MnO_3$ ceramics prepared by Plasma Activated Sintering, Mater. Res. Bull. 99 (2018) 73-78.

[20] J. Ma, M .Theingia, Q.M Chen, W.Z Wang, X. Liu, H. Zhang. Influence of synthesis methods and calcination temperature on electricalproperties of $La_{1-x}Ca_xMnO_3$ (x = 0.33 and 0.28) ceramics, Ceram. Int. 39 (2013) 7839-7843.

[21] Jessica R. Chocha, Pooja A. Chhelavda and J.A. Bhalodia, Calcination temperature effect on $La_{0.67}Ca_{0.33}MnO_3$ nanoparticle using simple citrate pyrolysis process,T. Indian. I. Metals. 64 (2011) 159-163.

[22] D.H. Manha, P.T. Phong, T.D. Thanh, L.V. Hong, N.X. Phuc, Low-fifield magnetoresistance of $La_{0.7}Ca_{0.3}MnO_3$ perovskite synthesized by reactive milling method, J. Alloy. Compd. 499 (2010) 131-134.

[23] L. Li, H. Zhang, X. Liu, P. Sun, C. Wang, X. Wang, B. Li, G. Liang, Q. Chen, Structure and electromagnetic properties of $La_{0.7}Ca_{0.3-x}K_xMnO_3$ polycrystalline ceramics, Ceram. Int. 45 (2019) 10558-10564.

[24] L.M. Wang, C.Y. Wang, C.C. Tseng, Correlation of the temperature coefficient of resistivity for doped manganites to the transition temperature, polaron binding energy, and magnetic order. Appl. Phys. Lett, 100 (2012) 232-403.

[25] J.S. Helman, B. Abeles, Tunneling of Spin-Polarized Electrons and Magnetoresistance in Granular Ni Films, Phys. Rev. Lett. 37 (1976) 1429-1432.

[26] M. Theingi, J. Ma, H. Zhang, X. Gao, J.H. Yi, Q.M. Chen, Study of structural and electrical transport properties of polycrystalline $La_{1-x}Ca_xMnO_3$ (x = 0.33 0.5, 0.9) prepared by a co-precipitation method, Adv. Mate. Res. 652 (2013) 576-780.

[27] A.M. Yang, Y.H. Sheng, M.A. Farid, H. Zhang, X.H. Lin, G.B. Li, L.J. Liu, F.H. Liao, J.H. Lin, Copper doped $EuMnO_3$: synthesis, structure and magnetic properties, RSC. Advs. 6 (2016) 13928-13933.

[28] H. Gencer, M. Pektas, Y. Babur1, V.S. Kolat, T. Izgi, S. Atalay, Electrical transport and magnetoresistance of $La_{0.67}Ca_{0.33}MnO_3$:Ag_x (x = 0, 0.1, 0.2, 0.3, 0.4) composites, J. Magn. 17 (2012) 176-184

[29] Y. Li, H. Zhang, Q. Chen, D. Li, Z. Li, Y. Zhang, Effects of A-site cationic radius and cationic disorder on the electromagnetic properties of $La_{0.7}Ca_{0.3}MnO_3$ ceramic with added Sr, Pb, and Ba, Ceram. Int. 44 (2018) 5378-5384.

[30] P. Schiffer, A.P. Ramirez, W. Bao, S.W. Cheong, Low temperature magnetoresistance and the magnetic phase diagram of $La_{1-x}Ca_x$MnO3, Phys. Rev. Lett. 75 (1995) 3336-3339.

[31] L. Liu, D. Shi, S. Zheng, Y. Huang, S. Wu, Y. Li, L. Fang, C. Hu, Polaron relaxation and non-ohmic behavior in $CaCu_3Ti_4O_{12}$ ceramics with different cooling methods, Mater. Chem. Phys. 139 (2013) 844-850.

[32] U. Aschauer, R. Pfenninger, S.M. Selbach, T. Grande, N.A. Spaldin, Strain controlled oxygen vacancy formation and ordering in $CaMnO_3$, Phys. Rev. B. 88 (2013) 3929-3940.

[33] L.W. Lei, Z.Y. Fu, J.Y. Zhang, H. Wang, K. Niihara, Low field magnetoresistance of $La_{0.7}Ca_{0.3}MnO_3$ ceramics fabricated by fast sintering process. J. Alloy. Compd. 530 (2012) 164-168.

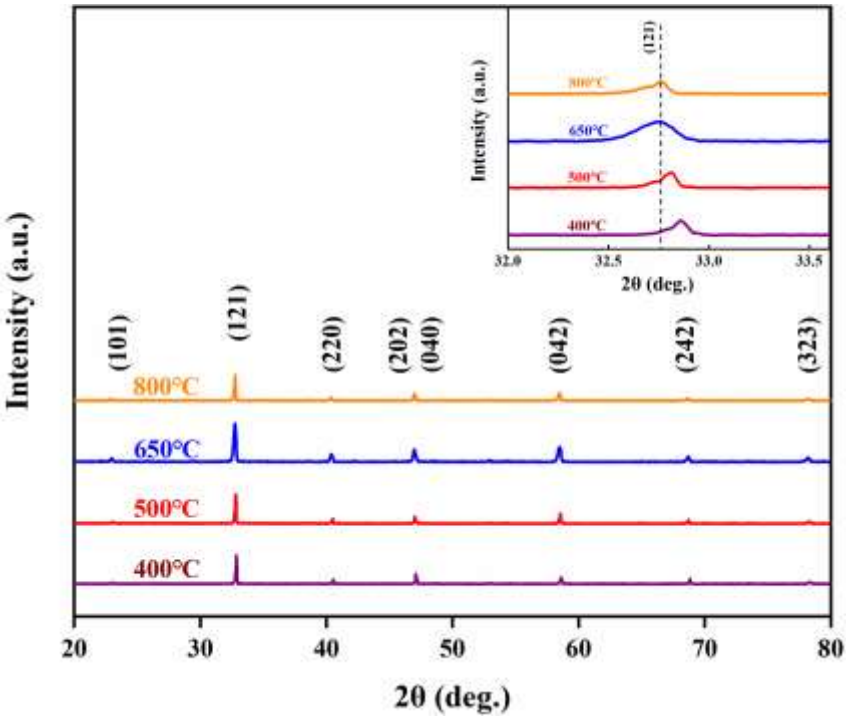

Fig. 1 *XRD* patterns of the LCMO samples calcinated at 400℃, 500℃, 650℃ and 800℃, Insets are the magnified view of the strongest diffraction peak.

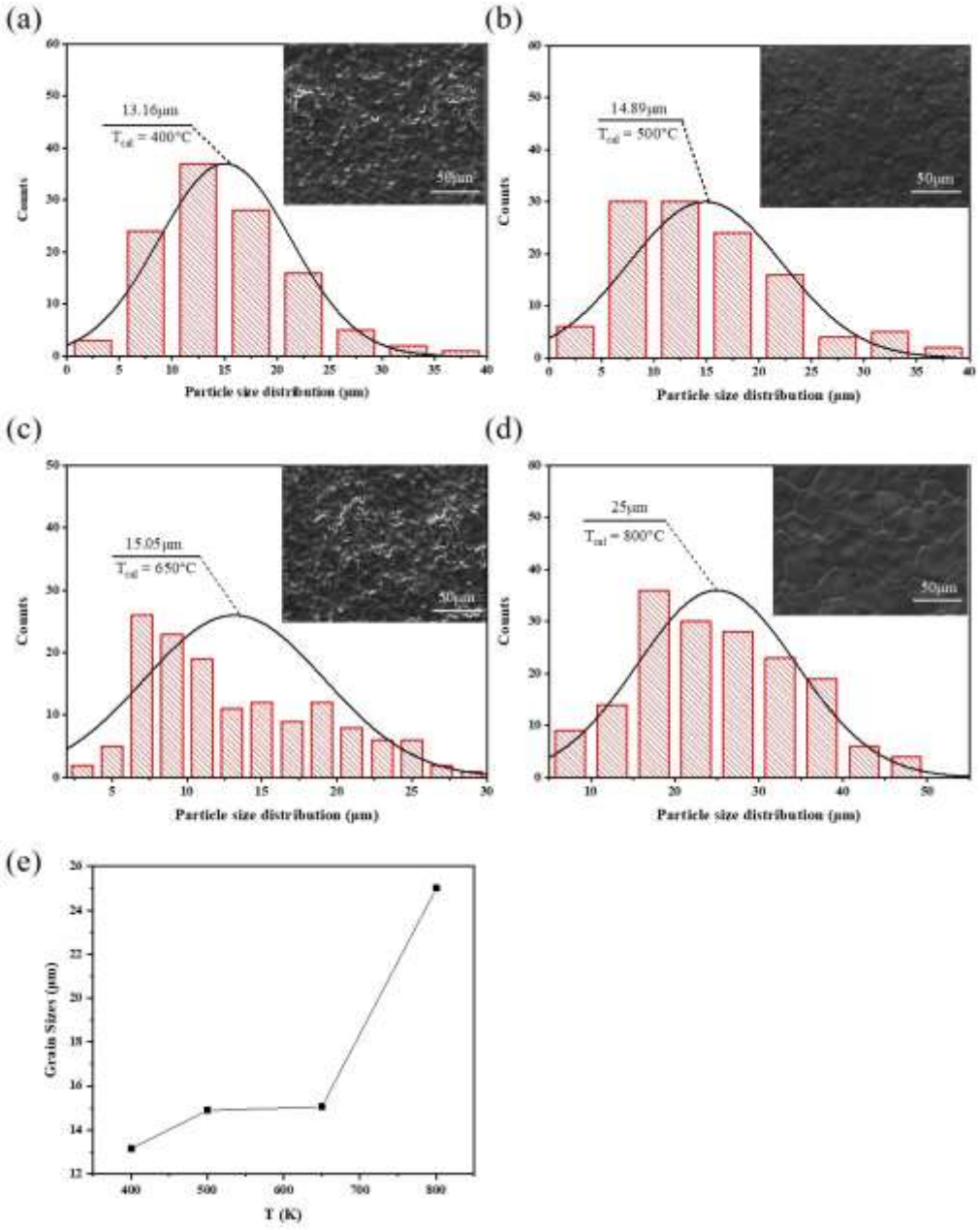

Fig. 2(a–d) *SEM* micrographs of LCMO samples calcinated at T_{cal} =400 ℃ (a), 500℃ (b), 650℃ (c), 800℃ (d). (e) Grain size with different T_{cal}.

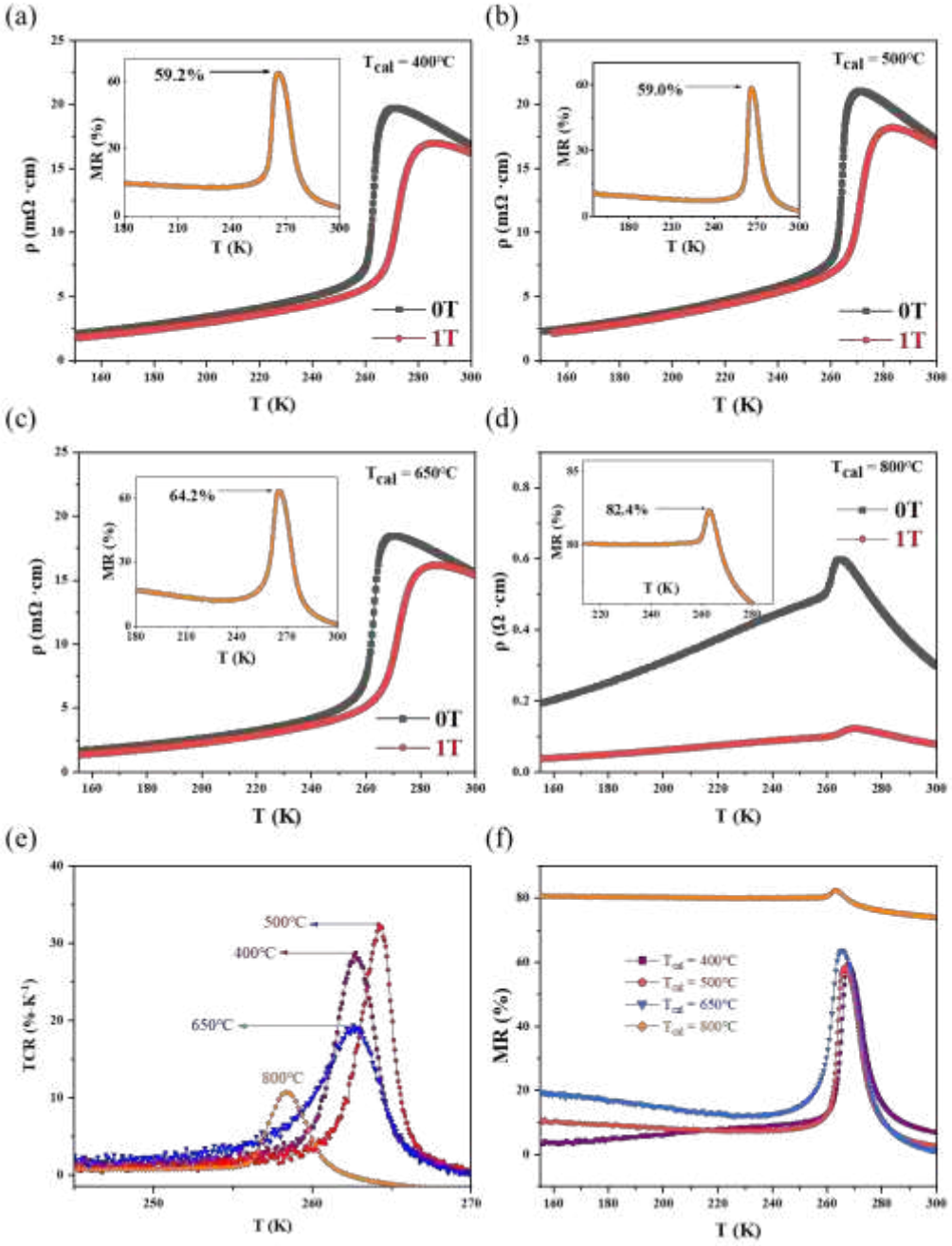

Fig. 3(a-d) Temperature-dependent resistivity of the LCMO ceramics calcinated at various temperatures. (e) Variation in *TCR* (% K^{-1}) with T_{cal} for LCMO composites.(f) Temperature-dependent magnetoresistance of the LCMO ceramics calcinated at various temperatures.

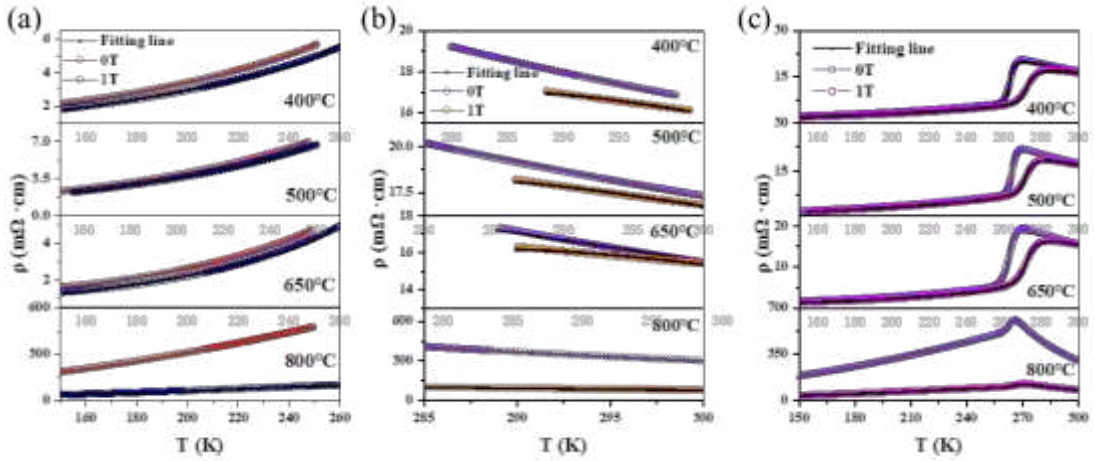

Fig. 4. Fit curves of electrical resistivity in different temperature rage (a) Low temperature range ($T < T_{MIT}$); (b) High temperature range ($T > T_{MIT}$); (c) Entire temperature range.

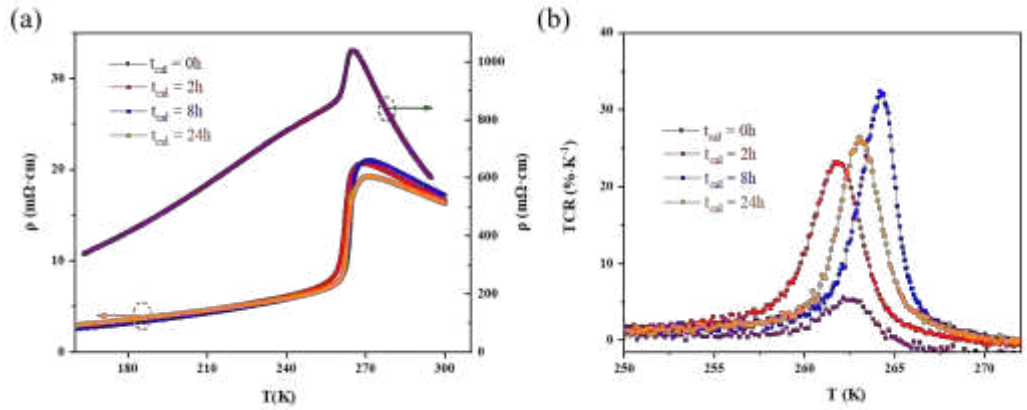

Fig.5 (a) Temperature dependence of resistivity when changing the t_{cal}; (b) Variation in *TCR* (% K^{-1}) with t_{cal} for LCMO composites.

Table 1. Structure and refinement parameters of LCMO samples.

Calcination temperature (℃)	**400**	**500**	**650**	**800**
Space group	*Pnma*	*Pnma*	*Pnma*	*Pnma*
a(Å)	5.4535	5.45830	5.45560	5.45430
b(Å)	7.7076	7.71250	7.70950	7.70970
c(Å)	5.4687	5.47280	5.47250	5.47200
Cell Volume V(Å^3)	229.8680	230.3892	230.1730	230.1031
d_{Mn-O1} (Å)	1.93515	1.93638	1.93563	1.93568
d_{Mn-O2} (Å)	1.06601	1.06597	1.06611	1.06616
Mn-O_1-Mn (°)	169.4153	169.4141	169.4106	169.4119
Mn-O_2-Mn (°)	161.1546	161.1550	161.1552	161.1548
R_e (%)	22.7410	22.3173	13.8386	23.1465
R_p (%)	14.7911	15.8047	10.1391	16.9739
R_b (%)	18.8926	19.5795	12.3135	20.3379

Table 2. Main electrical performance comparison of LCMO samples under different calcination temperature

Calcination temperature (℃)	T_{MIT} **(K)**	***TCR*** **(% • K^{-1})**	ρ_{max} **(Ω • cm)**	ρ_{296k} **(Ω • cm)**	**Shrinkage ratio (%)**
400	271.1	28.8	0.0197	0.0173	0.52
500	271.3	32.3	0.0210	0.0178	0.48
650	271.6	19.4	0.0159	0.0143	0.42
800	262.4	10.8	0.1325	0.0749	0.32

Table 3. Low temperature fitting parameters

Calcination temperature (℃)	**Field (T)**	ρ_0 **(Ω·cm)**	ρ_2 **(Ω·cm·K^{-1})**	$\rho_{4.5}$ **(Ω·cm·K^{-1})**	**R^2**
400	**0**	9.40E-04	4.42E-08	3.20E-14	0.99948
	1	8.46E-04	3.38E-08	3.05E-14	0.99851
500	**0**	8.45E-04	5.29E-08	3.78E-14	0.99932
	1	7.71E-04	4.77E-08	3.63E-14	0.99644
650	**0**	9.80E-04	1.52E-08	5.41E-14	0.99846
	1	1.03E-03	1.53E-09	4.55E-14	0.99959
800	**0**	2.47E-02	7.01E-06	2.25E-13	0.99932
	1	4.77E-03	1.80E-06	2.23E-13	0.99901

Table 4. *SPH* model fitting parameters

Calcination temperature (℃)	**Field (T)**	**E_a (meV)**	**R^2**
400	**0**	1.16E-20	0.99756
	1	9.34E-21	0.9982
500	**0**	1.29E-20	0.99656
	1	1.11E-20	0.99165
650	**0**	1.33E-20	0.99959
	1	9.18E-21	0.99644
800	**0**	2.79E-20	0.99972
	1	2.33E-20	0.99854

Table 5. Percolation model fitting parameters

Calcination temperature (℃)	**Field (T)**	$\frac{U_0}{k_B}$ **(K)**	$T_{c\text{-}mod}$**(K)**	**R2**
400	**0**	4.44E+04	2.64E+02	0.999
	1	2.56E+04	2.73E+02	0.99979
500	**0**	5.44E+04	2.65E+02	0.99919
	1	2.75E+04	2.73E+02	0.99973
650	**0**	3.33E+04	2.63E+02	0.99846
	1	2.48E+04	2.73E+02	0.99986
800	**0**	4.59E+04	2.64E+02	0.99833
	1	3.03E+04	2.69E+02	0.99879

Figures

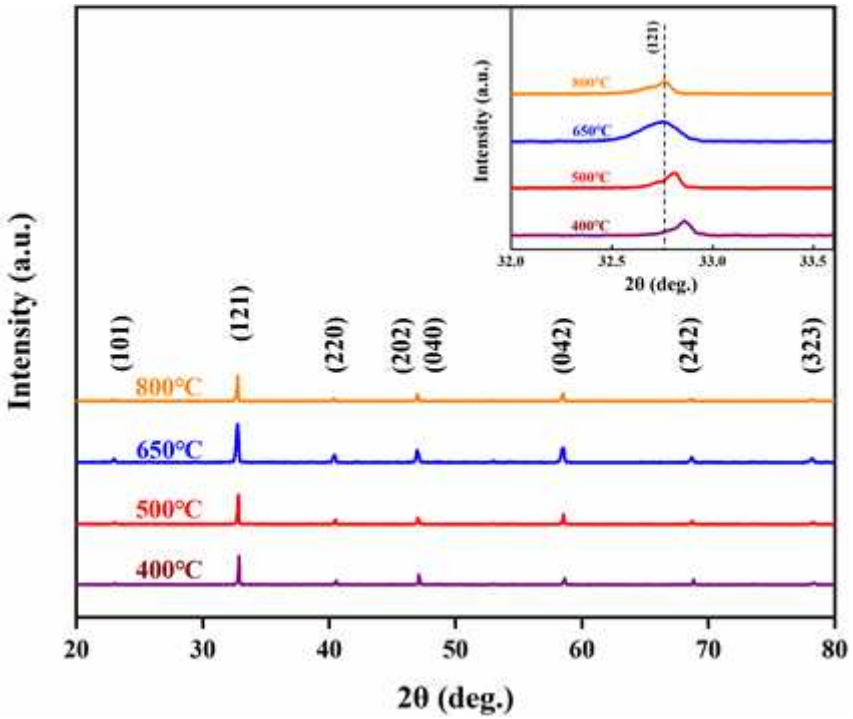

Figure 1

XRD patterns of the LCMO samples calcinated at 400℃, 500℃, 650℃ and 800℃, Insets are the magnified view of the strongest diffraction peak.

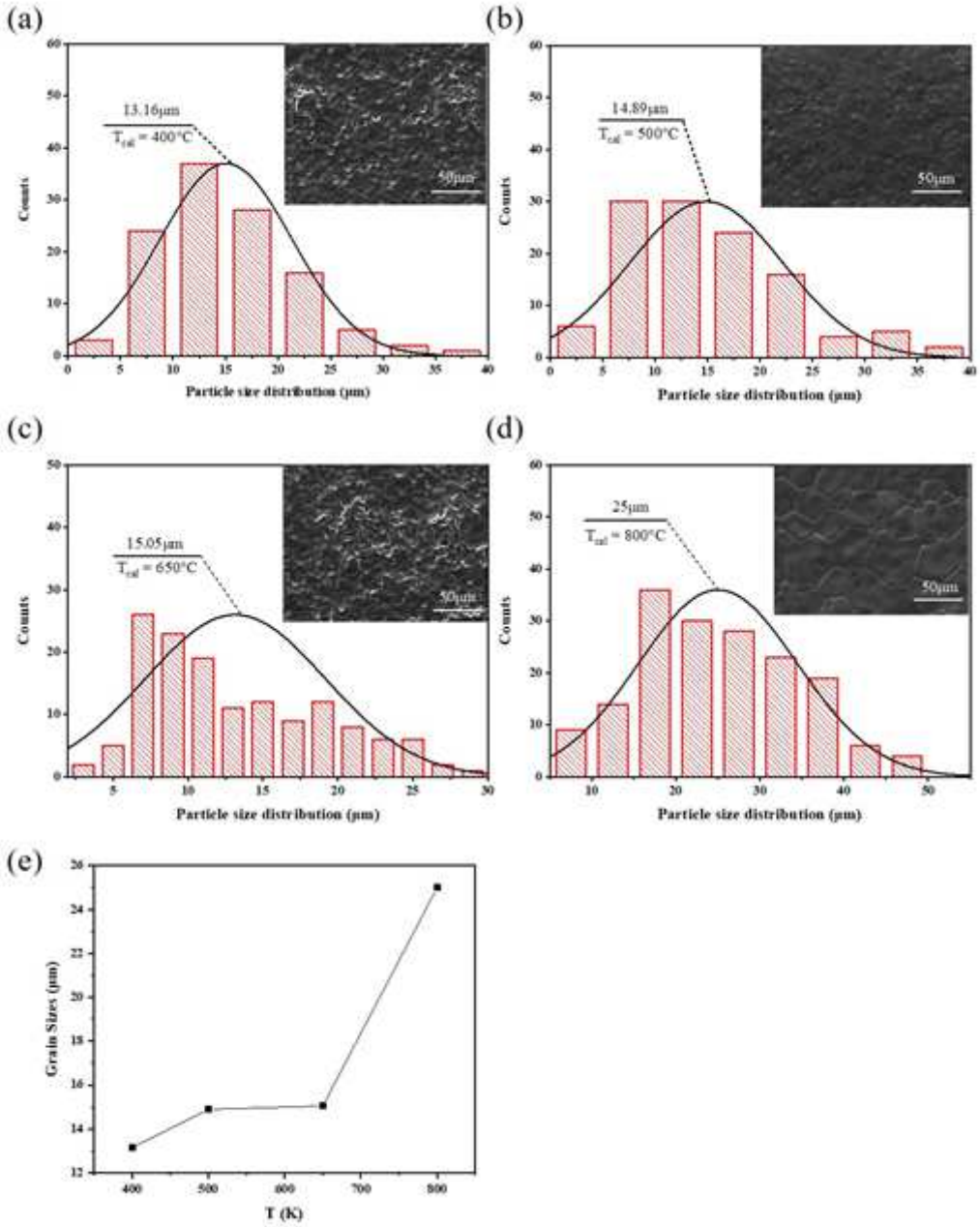

Figure 2

(a–d) SEM micrographs of LCMO samples calcinated at Tcal =400 ℃ (a), 500℃ (b), 650℃ (c), 800℃ (d). (e) Grain size with different Tcal.

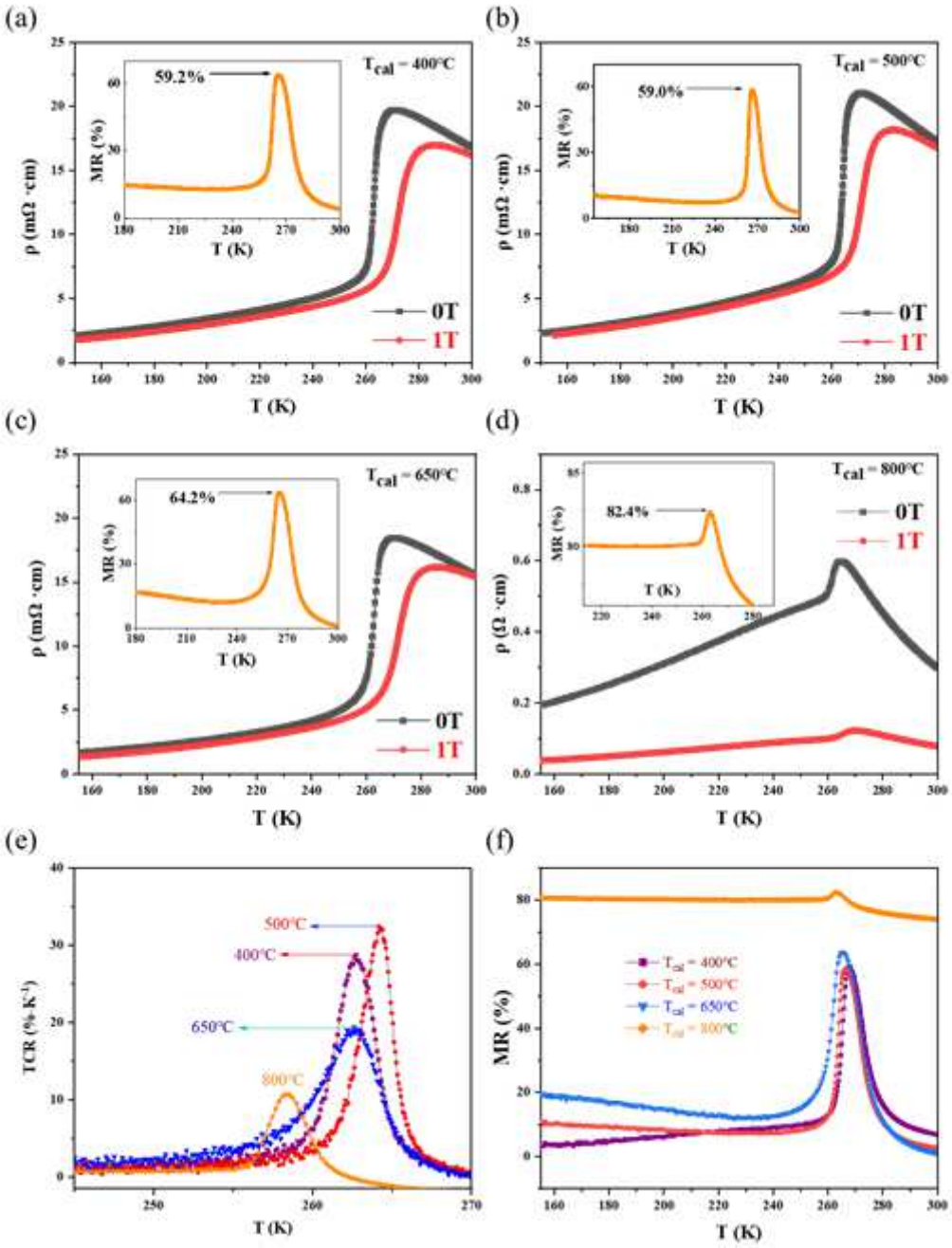

Figure 3

(a-d) Temperature-dependent resistivity of the LCMO ceramics calcinated at various temperatures. (e) Variation in TCR (% K−1) with Tcal for LCMO composites.(f) Temperature-dependent magnetoresistance of the LCMO ceramics calcinated at various temperatures.

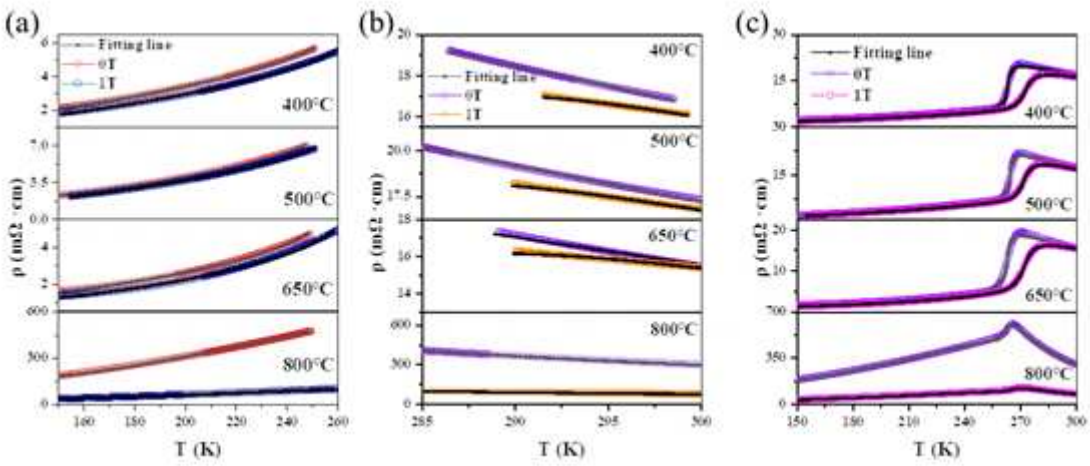

Figure 4

Fit curves of electrical resistivity in different temperature rage (a) Low temperature range (T < TMIT); (b) High temperature range (T > TMIT); (c) Entire temperature range.

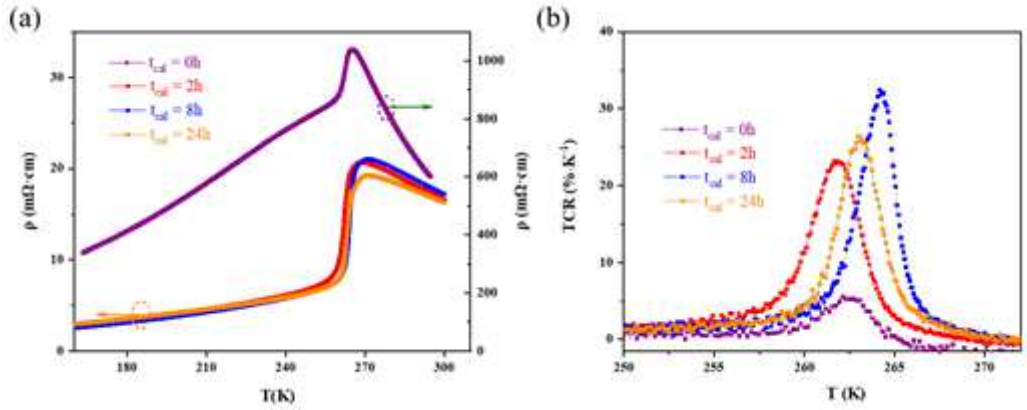

Figure 5

(a) Temperature dependence of resistivity when changing the tcal; (b) Variation in TCR (% K−1) with tcal for LCMO composites.